MECHANISM OF MODULATED ELECTRO-HYPERTHERMIA INDUCED TUMOR GROWTH SUPPRESSION IN B16F10 MELANOMA PULMONARY METASTASES

PhD thesis

Thomas Mbuotidem Jeremiah

Theoretical and Translational Medicine Doctoral School

Semmelweis University

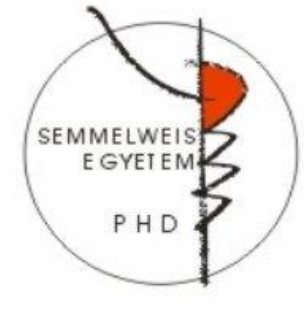

Supervisor: Zoltán Benyó, MD, D.Sc.

Official reviewers: Eleonóra Nardainé Imrédi, MD, Ph.D.
Zoltán Lohinai, MD, Ph.D.

Head of the Complex Examination Committee: György Losonczy, MD, D.Sc.

Members of the Complex Examination Committee: Lajos Géczi, MD, Ph.D.
Kulka Janina, MD, D.Sc.

Budapest

2021

1. Introduction

Metastatic dissemination of cutaneous melanoma to subcutaneous tissues, locoregional lymph nodes, and distant organs and tissues is common. The lung is by far the most common site of distant metastases of melanoma. Lung metastases of melanoma predict a very poor prognosis with a 5-year survival rate of less than 10% (1, 2). Several treatments have been approved by the United States Food and Drug Administration (FDA) in recent years for melanoma treatment. The treatment options may be surgical excision, radiotherapy, chemotherapy, photodynamic therapy, or immunotherapy depending on the tumor's characteristics such as genetic profile, stage, and location (3). Hyperthermic therapies including modulated electro-hyperthermia (mEHT) have been used to enhance the efficacy of chemotherapy, radiation therapy, and, recently, immunotherapy of tumors (4). mEHT capacitive coupling creates an electromagnetic field that is predominantly absorbed in the tumor relative to adjacent normal tissues (5)**.** Tumor cells demonstrate increased glucose uptake due to the Warburg effect, thus, resulting in an enhanced buildup of lactate, accompanied by an increased metal ion, and salt content (6), leading to increased conductivity and dielectric permittivity (7). This increases selective absorption of the electromagnetic field by tumors, leading to increased heat generation within the tumor mass. mEHT therapy has been demonstrated to induce substantial apoptosis and decreased tumor proliferation in glioma cultures (8). In colorectal adenocarcinoma models, mEHT treatment has been demonstrated to induce both caspase-dependent and caspase-independent AIF-mediated apoptosis (9-11). B16 melanoma is a C57BL/6-derived highly aggressive variant of melanoma with high metastatic capability from subcutaneous location to lungs. Intravenous injection of B16F10 is a member of the B16 melanoma tumor cell line with high metastatic capability that readily results in metastatic colonization of the lungs (12)**.** This makes it a suitable tumor model for our experimental studies. In this study, we focus on the optimization of mEHT as a novel treatment modality for the targeted treatment of lung tumors in mice. Furthermore, we investigated the means and mechanisms of the anti-tumor effect of mEHT on B16F10 melanoma.

2. Objective

Although the efficacy of mEHT has been described extensively in multiple primary tumor models in mice, studies on the applicability and efficacy of mEHT as a viable treatment option in a pulmonary metastatic model have not been described before. This is probably due in part to the complexity of the thorax and the difficulty it poses to the application of mEHT as a treatment option. Additionally, the lack of adequate devices optimized for the targeted treatment of lung tumors presents a particular problem. Another challenging aspect of mEHT application in lung treatment is the difficulty of measuring lung temperature during treatment as direct measurement poses a significant risk of mechanical lung injury.

Therefore, in this study, we aimed at:

1. Developing a device-optimized-treatment-technique for targeted mEHT treatment of lung tumors.
2. Developing a minimally invasive method of indirect lung temperature measurement during mEHT treatment of lung tumors in mice.
3. Verifying the efficacy of mEHT on B16F10 melanoma in a subcutaneously induced primary tumor and pulmonary metastases model following the usual pattern of clinical dissemination of melanoma from the skin to the lungs.
4. Investigating the underlying molecular mechanisms of tumor growth inhibition by mEHT in a B16F10 melanoma pulmonary metastases model.
5. Investigating the capability of mEHT treatment-induced immune cells mobilization.
6. Investigating auxiliary lung damage as a potential adverse event following mEHT treatment of lungs in mice.

3. Materials and Methods

3.1. Animals and cell lines

All procedures were carried out according to the guidelines of the Hungarian Law of Animal Protection (28/1998) and were approved by the Government Office of Pest County (Permission number: PE/EA/50-2/2019 and PE/EA/51-2/2019). Animals tested in this study were the offspring of C57BL/6 colonies grown in the animal facility of the

Semmelweis University. B16F10 mouse melanoma cell line (ATCC® CRL 6475™) was purchased from ATCC (Manassas, VA, USA). Cells were cultured in minimum essential medium (MEM) supplemented with 1% (v/v) MEM-vitamin solution, 5% (v/v) heat-inactivated HyClone fetal bovine serum, 1 mM sodium pyruvate, 2 mM L-glutamine and 1% (v/v) nonessential amino acids (NEAAs) purchased from Thermo Fisher Scientific (Waltham, MA, USA).

3.2. PET imaging and data analysis

In vivo positron emission tomography (PET) experiments were conducted at the Department of Biophysics and Radiation Biology, Semmelweis University. Animals were fasted before the experiment for 6 hours. Prior to PET imaging, 12-18 MBq radioactivity of [^{18}F]FDG (FDG-KEDOI® injection, Pet-Medicopus Ltd, Kaposvár, Hungary) in 0.2-0.3 mL was injected into the tail vein of the animals. After 90 min of post-injection awake [^{18}F]FDG uptake period, animals were anesthetized with 1.5% isoflurane in medical oxygen. During anesthesia, animals were placed in an immobilizing animal bed (MultiCell, Mediso, Budapest, Hungary). Static, 15 min PET whole-body scans of animals were performed using a microPET P4 scanner (Concorde Microsystems, US). Image volumes from the collected list mode data were then reconstructed using the instrument`s dedicated three-dimensional maximum a posteriori algorithm with a 1.56 mm voxel size. Data evaluation was carried out using two dedicated small animal image analysis software, Fusion (Mediso, Budapest, Hungary) and vivoQuant (inviCRO, MA, US). Three-dimensional lung regions of interest were drawn using a connected threshold algorithm, while blood regions of interest were manually drawn around the left ventricle of the heart. For the calculation of the Tumor Maximal Standardized Uptake Ratio (SURmax), and SUVmax, the standardized uptake values (SUV) were estimated by the following equation: [tissue concentration (MBq/mL) x the body weight (g)]/injected dose (MBq). Thereafter, SURmax was obtained by time correcting the ratio of lung maximal SUV value in the lung region of interest (SUVmax) to blood SUV multiplied by the ratio of 75 min post-injection to 90 min post-injection, as described by Hofheinz et al. (13-15). After calculations, all mouse PET quantitative data were normalized to the respective lung mass (in grams) of each animal to account for initial size-related vascularization-derived differences in signal.

3.3. *In vivo* mEHT treatment

In the metastatic tumor model, pulmonary metastases of melanoma were established by injecting 10^5 B16F10 melanoma cells *via* tail vein into seven-to-nine-week-old female C57BL/6 mice. The animals were treated using the LabEHY-200 device (Oncotherm Ltd., Páty, Hungary). All animals were placed between the circuit's plane-parallel asymmetric electric condensers during treatment. The circuit consisted of a 72-cm^2 aluminum electrode which served also as a heating pad used to maintain the physiological temperature of the animal at approximately 37 °C . The impedance was precisely matched, and the electromagnetic field was generated at 13.56 MHz radiofrequency using 1/f amplitude modulation. The upper conductive textile chest electrode was placed on the chest overlying the tumor-burdened lungs. Treatment with the lung-optimized chest electrode was repeated every third day for a total of six times for 30 min each starting from day 1. mEHT ability to induce heat-stress and DAMP signal release of B16F10 melanoma cells was verified in a primary solid B16F10 melanoma tumor model. In the primary tumor model, melanoma tumors were established by mixing 10^6 B16F10 cells with growth factor reduced matrigel (Trevigen, Gaithersburg, MD, USA) injected subcutaneously into seven-to-nine-week-old female C57Bl/6 mice in the right inguinal area. An upper pole electrode was positioned over the growing tumor in the right inguinal region. The first mEHT treatment of 30 min was performed on day 4 after the implantation of the tumor cell/matrigel mixture and was repeated two more times with one day in between treatments. Animals were anesthetized with 2% isoflurane during treatment. Animals were housed separately, and treated control animals were maintained under similar conditions. Animals tested in this study were the offspring of C57BL/6 colonies grown in the animal facility of Semmelweis University, Budapest, Hungary. All animal work conducted during this study was approved by the Governmental Ethical Committee under the permission number PE/EA/51-2/2019.

3.4. Immunohistochemistry

Lung tissues fixed in 10% neutral buffered formalin were dehydrated and embedded in paraffin. 2.5 μm thick serial sections were cut, mounted on silanized glass slides, and kept in a thermostat at 65 °C for 1 hour. Sections were dewaxed and rehydrated for hematoxylin-eosin (H&E) staining, Masson’s trichrome staining, and

immunohistochemistry (IHC). For antigen retrieval, sections were heated for 20 min in Tris-EDTA (TE) buffer pH 9.0 (0.1 M Tris_base and 0.01 M EDTA) using an Avair electric pressure cooker (ELLA 6 LUX D6K2A, Bitalon Kft, Pécs, Hungary) followed by a 20 min cooling with an open lid. Endogenous peroxidases were blocked using 3% H_2O_2 in methanol while non-specific proteins were blocked with 3% bovine serum albumin (BSA, #82-100-6, Millipore, Kankakee, Illinois, USA) diluted in 0.1 M Tris-buffered saline (TBS, pH7.4) containing 0.01% sodium-azide, both for 15 min. The sections were incubated with primary antibodies (Table 2) diluted in 1% BSA/TBS+TWEEN (TBST, pH 7.4) overnight in a humidified chamber. Peroxidase conjugated anti-rabbit & anti-mouse IgGs (HISTOLS-MR-T, micropolymer -30011.500T, Histopathology Ltd., Pécs, Hungary) were used for 40 min incubations and the enzyme activity was revealed by 3,3'-diaminobenzidine (DAB) chromogen/hydrogen peroxide kit (DAB Quanto, #TA-060-QHDX, Thermo, WA, USA) under microscopic control. All incubations were done at room temperature with samples washed between incubations in TBST buffer for 2 x 5 minutes. Digitalization of slides and evaluation of immune reactions were done using modules of the QuantCenter image analysis software tool pack (3DHISTECH, Budapest, Hungary). As multiple pulmonary melanoma nodules were noted in each lung sample, all tumors in each section were annotated for subsequent evaluations. The portion of p-H2Axγ(Ser139), CCasp3, and $p21^{waf1}$, Ki67(SP6), F4/80 (D2S9R), CD3, CD8α (D4W2Z) positive cells were quantified as a percentage of the total annotated tumor areas (HistoQuant module) while the portion of MPO positive cells and Masson's trichrome positive area was quantified as a percentage of the total lung area. Evaluation of histological lung injury was performed as described by Ehrentraut et al (16) taking into consideration scores of individual components of cellular inflammatory cell infiltrates in air space or vessel wall (1 = only wall; 2 = one to five cells (few cells) in air space; 3 = intermediate; 4 = severe (congestion of air space)), interstitial congestion and hyaline membrane formation (1 = normal lung; 2 = moderate (<25% of lung section); 3 = intermediate (25–50% of lung section); 4 = severe (>50% of lung section)), hemorrhage (0 = absent; 1 = present). From each animal, a total of six representative images were analyzed using a blinded semi-quantitative scoring system.

Table 1. Antibodies and conditions used for immunohistochemistry

Antigen	Type	Reference no.	Dilution	Antigen retrieval	Vendor
p-H2Axγ(Ser139)	Rabbit, mAb	#9718	1: 200	T-E	Cell Signaling
CCasp3	Rabbit, pAb	#9664	1:100	Citrate	Cell Signaling
$p21^{waf1}$	Rabbit, mAb	#ab188224	1:300	T-E	Abcam
Ki67 (SP6)	Rabbit, mAb	#MA5-14520	1:100	T-E	Thermo
F4/80 (D2S9R)	Rabbit, mAb	# 70076	1:300	T-E	Cell Signaling
CD3	Rabbit, pAb	#IS503	1:3	T-E	Dako
CD8α (D4W2Z)	Rabbit, mAb	#98941	1:500	T-E	Cell Signaling

(Vendor specification: Cell Signaling (Danvers, MA, USA); Thermo (Waltham, MA, USA); Dako (Glostrup, Denmark); Abcam (Cambridge, UK); Sino Biological (Beijing, China); T-E: Tris-EDTA, pH 9.0)

3.5. Measurement of extracellular hsp70, HMGB1, and ATP

The tumor interstitial fluid was obtained by digesting tumors as described above. After removing cells by centrifugation, the supernatant was further purified by centrifugation at maximum speed for 10 min and stored at -70 °C until use. The protein concentration of the tumor effusate was measured using Bradford reagent (Thermo Fisher Scientific). In the subsequent measurements, an equal amount of protein was used. The heat shock protein 70 (hsp70) concentration was measured using an hsp70 High-Sensitivity ELISA kit (Abcam). The high-mobility group protein B1 (HMGB1) concentration was determined using a specific ELISA kit from Aviva Systems Biology (San Diego, CA, USA) following the manufacturer's protocol. Absorbance was measured at 450 nm with a PowerWave microplate spectrophotometer (BioTek, Winooski, VT). ATP content was evaluated using a luciferase-based ATP determination kit (Thermo Fischer Scientific) following the manufacturer's instructions. Luminescence was measured with a Varioskan Flash microplate reader (Thermo Fischer Scientific).

3.6. Statistical analysis

Statistical analysis was performed using GraphPad Prism software (v.6.07; GraphPad Software Inc., La Jolla, CA, USA). The normality of data distribution was assessed using the Kolmogorov-Smirnov test and an unpaired t-test or Mann-Whitney nonparametric test

was performed accordingly for determination of significance. Data are expressed as mean ± SE, $p < 0.05$ were considered as significant.

4. Results

4.1. mEHT suppressed primary tumor growth of B16F10 melanoma

Prior to investigating the effect of mEHT on a pulmonary melanoma metastatic model, we first evaluated whether mEHT can have a significant tumor growth inhibition effect on B16F10 melanoma in a primary tumor model, primarily due to the simplicity of the model in comparison to the more complex pulmonary metastatic model. 10^6 B16F10 cells mixed with growth factor reduced matrigel (Trevigen, Gaithersburg, MD, USA) was subcutaneously injected into seven-to-nine-week-old female C57Bl/6 mice in the right inguinal area, simulating a primary tumor model. Before performing treatments, we set up conditions providing a standard 42 °C intra-tumoral temperature in a series of animals. The temperature was monitored using optical thermo-sensors inside tumors, rectally, subcutaneously, and directly below the upper electrode to assess the thermal effect in and around treated tumors. The power adjustment profile allowed accurate maintenance of temperature around 42 °C in the center of the treated grafts. The subcutaneous temperature was 1 °C lower than the tumor center, while the skin surface was 39 °C, indicating a thermal gradient, with the highest value in the tumor core. The duration of the treatment was 30 min, following common clinical practice in mEHT application. Using this protocol, relying solely on the skin surface and rectal temperature measurements, we demonstrated that mEHT treatment resulted in significant tumor weight reduction after three-time treatments.

4.2. mEHT induced localized temperature increase in mice lung

As mEHT has not been used before for interventions in the lung, our first objective was to develop a suitable chest electrode capable of inducing lung-specific hyperthermia without treatment-associated damage to nearby structures such as the heart, liver, and skin in mice. Because the impedance of the lung to transmitted energy is far higher than that of the neighboring tissues, the electrode needed to cover exclusively the target area, thereby avoiding the dissipation of energy to nearby structures. Based on these considerations, several chest electrodes were designed and tested for inducing lung-

specific hyperthermia with a targeted treatment temperature range of 41.5 – 42.0 °C and the upper conductive textile chest electrode shown in Figure 1A (right panel) and 1B was found to be optimal for lung treatment.

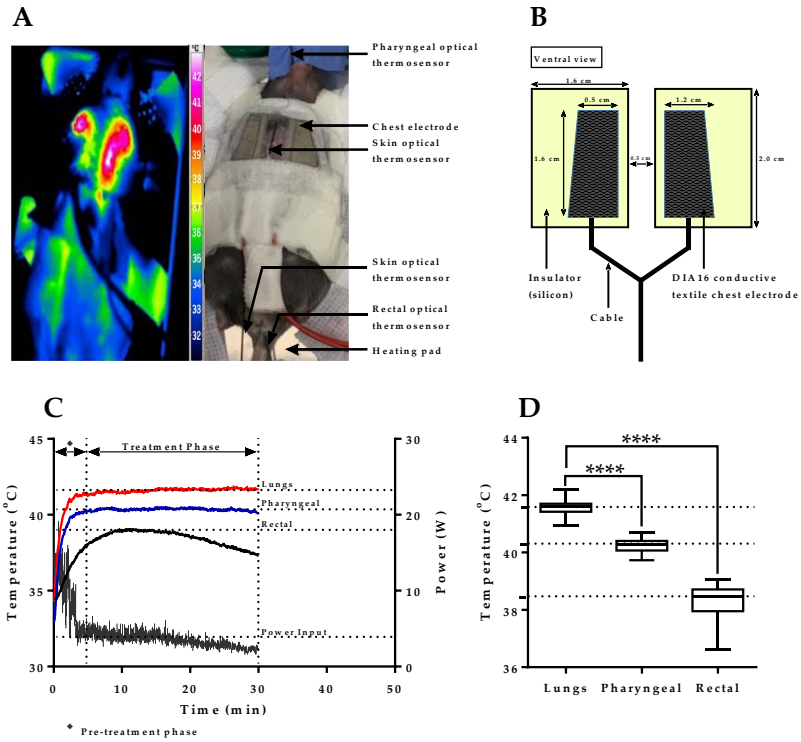

Figure 1. Localization of heat stress during targeted mEHT treatment of lungs. (A) Thermal image depicting a localized increase in temperature over target area on mice thorax (left panel) and treatment layout with the positioning of chest electrode and optical thermosensors (right panel); (B) Dimensions of conductive textile chest electrode for targeted lung treatment of tumors in mice; (C) Plot depicting temperature profiles of lungs, pharynx, and rectum with applied power settings; (D) Pharyngeal and rectal temperature versus lung temperature in treatment phase (n=4). Data represent average ± SEM. Mann-Whitney test, ****$p < 0.0001$.

We demonstrated a localized increase in temperature over the target area on mice chest as represented by the externally measured thermal mapping shown in Figure 1A (left panel). Figure 1B depicts the dimensions of the conductive textile chest electrode used in this study for the targeted treatment of lung tumors in mice. Figure 1C shows the power adjustment profile of mEHT with measured lungs, pharyngeal, and rectal temperatures at different time points. A significant difference was observed between measured lung/pharyngeal and lung/rectal temperatures ($p<0.0001$) with mean temperature values of 41.6 ± 0.1 °C, 40.3 ± 0.1 °C, and 38.5 ± 0.5 °C measured in the lung, pharynx, and rectum respectively during treatment (Figure 1D). These results

demonstrate that the targeted temperature range for mEHT treatment of lungs could be achieved with the current chest electrode while maintaining limited dissipation of energy to nearby structures and the whole body.

4.3. Minimally invasive technique of lung temperature measurement in mEHT

The accurate measurement of lung temperature during repeated treatments with mEHT is highly essential to ensure that targeted treatment temperature is reached but not exceeded. Direct lung temperature measurement, however, is not feasible partly due to the high risk of mechanical lung injury. Therefore, we sort out to develop a minimally invasive method of estimating lung temperature during mEHT treatment in mice. Optical thermosensors were advanced into the main bronchi, pharynx, and rectum of non-tumor-bearing animals and treated with mEHT for 30 min. Access to mice trachea was enabled *via* puncture tracheotomy through which an optical thermosensor was advanced to the lung's main bronchi and *via* oral access, a pharyngeal optical thermosensor was placed in the pharynx of mice. Lung temperature was maintained at 41.5 – 42.0 °C using the power adjustment profile of mEHT and the pharyngeal temperature was monitored simultaneously. The objective here was to assess if a quantitative relationship exists between the lung and pharyngeal temperature; in which case, if a relationship is established, lung temperature could be estimated indirectly in subsequent experiments by measuring the pharyngeal temperature only. The average temperature difference observed between the lungs and pharynx measured in the treatment phase (5 – 30 min) was 1.3 ± 0.1 °C. This implies that by maintaining the pharyngeal temperature at 1.3 ± 0.1 °C lower than the targeted lung temperature of 41.5 – 42.0 °C, heat stress can be monitored and controlled less invasively in subsequent experimental treatment of lung tumors in mice. Following these experiments, subsequent treatment of tumor-bearing lungs was conducted by measurement of the pharyngeal temperature only eliminating the need for direct lung temperature measurement.

4.4. mEHT induced reduction of pulmonary metastatic burden in mice lungs

To define the potential impact of mEHT in the host lung on the development of metastatic nodules, 10^5 B16F10 melanoma cells were injected into the tail vein of seven-to-nine-week-old female C57BL/6 mice. All animals were treated six times using mEHT. The first mEHT treatment of 30 min was performed one day after the tail vein injection of the animals with B16F10 melanoma cells. Treatment was repeated every third day for a total of six times as defined by the experimental protocol (Figure 2A).

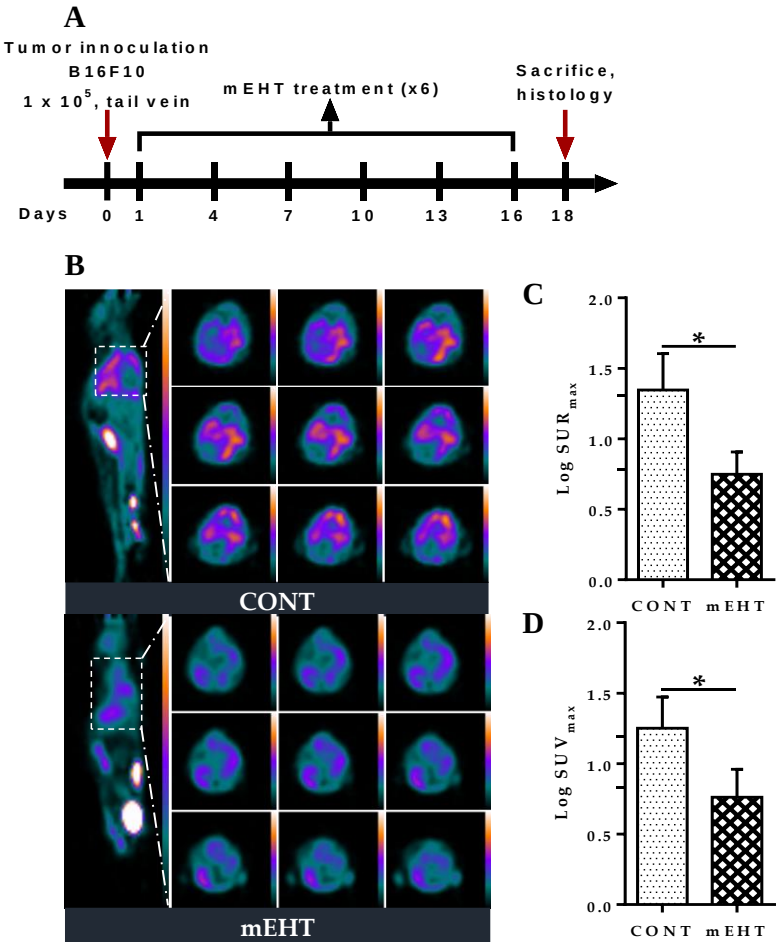

Figure 2. Effect of modulated-electrohyperthermia on tumor burden in mouse lungs. (A) Schematic representation of the experimental protocol; (B) Representative PET images depicting [^{18}F]FDG uptake in sagittal and coronal sections of CONT and mEHT; (C) Standardized uptake ratio (SURmax) of [^{18}F]FDG in CONT (n=4) and mEHT (n=3); (D) Standardized uptake value (SUVmax) of [^{18}F]FDG in CONT (n=4) and mEHT (n=3). Data represent average ± SEM. CONT vs mEHT, Mann-Whitney test. *$p < 0.05$.

Before sacrifice on day 18, PET imaging was performed on all animals to investigate the in vivo characteristics of mEHT-treated and sham-treated melanoma in mice lungs. Figure 2B shows representative PET images depicting [^{18}F]FDG uptake in sagittal and coronal sections of mEHT-treated and sham-treated control mice. As depicted by Figure 2C and 2D, significantly reduced SURmax ($p = 0.0169$) and SUVmax ($p = 0.0300$) were observed in the mEHT-treated lungs compared to the sham-treated ones.

Furthermore, a post-imaging sacrifice of all animals was performed to assess the gross pathological and metastatic burden of the lungs in both experimental groups. Visible tumor nodules were observed in the lungs of both mEHT-treated and sham-treated animals, indicating that metastatic tumors were successfully induced in mice lungs (Figure 3A). The pulmonary metastatic burden was assessed by counting the number of tumor nodules on the lung surface. Mice in the mEHT-treated group displayed a significantly lower number of tumor nodules (average of 17), whereas numerous distinguishable melanoma nodules (average of 60) were observed in the lungs of sham-treated animals ($p = 0.0049$, Figure 3B). In addition, excised lungs were weighted to further characterize the difference in tumor burden between the treated and control group. As shown in Figure 3C, the mean lung weight in the mEHT-treated group was significantly reduced indicating the suppression of tumor growth compared to the control group ($p = 0.0090$). Furthermore, analysis of H&E stained sections was performed to characterize mEHT-related tumor growth suppression in the lungs including intra-parenchymal tumors with no surface visibility which often proves difficult to quantify by surface tumor nodules evaluation only. Multiple focal lesions with pleomorphisms and marked cellular atypia were observed in both mEHT-treated and sham-treated lungs. Focal metastatic lesions in treated animals were significantly reduced in number especially for lesions < 0.1 mm^2 ($p = 0.0032$). Likewise, the number of focal lesions > 0.1 mm^2 was significantly reduced in treated lungs compared to the sham-treated ones ($p = 0.0497$,). Additionally, counts per unit lung area of focal lesions showed a significant reduction in mEHT-treated animals compared to the sham-treated ones ($p = 0.0039$). The total tumor area of focal metastatic melanoma lesions in mEHT-treated lungs was reduced significantly ($p = 0.0383$), although the relative area occupied by these lesions per lung showed marked reduction without reaching a statistically significant value ($p = 0.0968$).

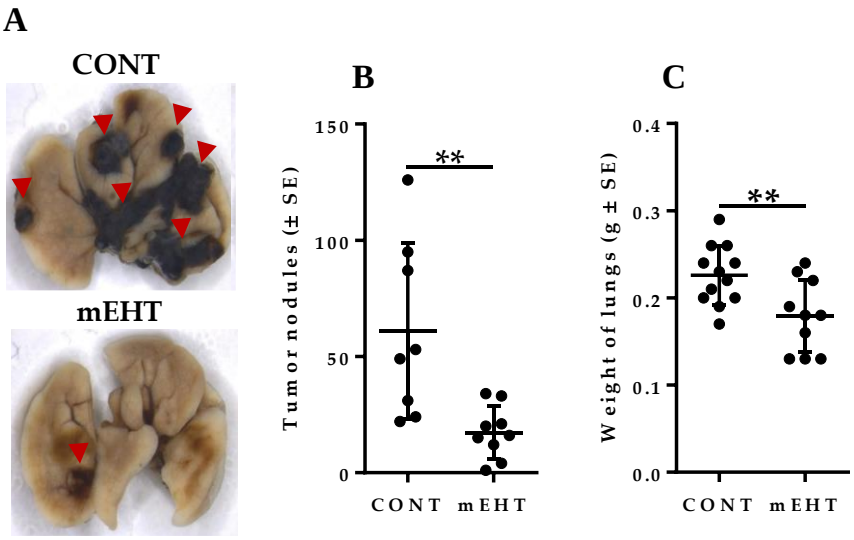

Figure 3. Effect of modulated-electrohyperthermia on tumor burden in mouse lungs. (A) Native lungs with pulmonary melanoma metastases in CONT and mEHT-treated animals; (B) Quantification of pulmonary melanoma metastatic nodules in CONT (n=8) and mEHT (n=9); (C) Quantification of lung weight in CONT (n=12) and mEHT (n=10). Data represent average ± SEM. CONT vs mEHT, unpaired t-test, **p < 0.01.

4.5. mEHT induced reduction in Ki67 expression in B16F10 melanoma cells

The depletion of Ki67 in some human tumor cell lines and primary fibroblast cells has been demonstrated to slow entry into the S-phase and coordinately downregulate genes involved in DNA replication thereby slowing the proliferation of tumor cells (17). Therefore, we investigated whether Ki67 downregulation plays a role in mEHT-mediated inhibition of B16F10 melanoma growth in murine lungs. Ki67 expression was measured by immunohistochemistry with anti-Ki67 antibody in both mEHT-treated and sham-treated tumors. Our investigation showed that Ki67 protein expression per unit tumor area was significantly reduced in mEHT-treated tumors compared to the control group ($p = 0.0085$).

4.6. mEHT induced cell cycle arrest in B16F10 melanoma cells

$p21^{waf1}$ is a potent cyclin-dependent kinase inhibitor, the upregulation of which coincides with increased cell cycle arrest and senescence (18). Therefore, we investigated the effect of mEHT on the nuclear expression and localization of $p21^{waf1}$ in treated B16F10 melanoma cells. mEHT-treated and sham-treated samples were stained for $p21^{waf1}$ *via* immunohistochemistry and analyzed using modules of the QuantCenter image

analysis software tool pack (3DHISTECH) for quantification. In mEHT-treated tumors, significant upregulation in $p21^{waf1}$ expression and nuclear localization was observed. The fraction of $p21^{waf1}$ positive cells as a percentage of tumor area was significantly increased in mEHT-treated tumors ($p = 0.0206$) compared to the sham-treated group.

4.7. mEHT induced DNA damage response in B16F10 melanoma tumor

Cellular response to DNA damage leads to a series of events, one of which is the phosphorylation of H2AX (19). H2AX phosphorylation typically occurs immediately after a DNA break formation, resulting in the recruitment of clusters of DNA damage response proteins at the site of damage, forming a DNA damage response focus (20). We tested the expression of phosphorylated H2AX (γ-H2AX) proteins to investigate whether mEHT induces significant DNA damage in treated tumors. While treated tumors showed marked DNA damage response to mEHT-treatment, adjacent normal lung tissue did not demonstrate any visible signs of DNA damage, reiterating that mEHT-associated DNA damage is confined only to the highly proliferating melanoma cells without associated damage to normal lung tissue. In treated tumors, the expression of γ-H2AX was significantly increased after six-time treatment with mEHT compared to the sham-treated group ($p = 0.0061$). Additionally, as DNA damage may lead to either cell senescence or programmed cell death (19), we investigated the role of apoptosis in mEHT-mediated inhibition of tumor growth and proliferation. Treated B16F10 melanoma cells demonstrated a comparable level of cleaved caspase 3 expression per tumor area as sham-treated ones with no significant difference between both groups ($p = 0.2331$).

4.8. mEHT induced DAMP signal release in B16F10 melanoma cells

To assess the ability of mEHT to induce DAMP signal release from B16F10 melanoma tumor, we isolated tumor interstitial fluid derived from mEHT-treated primary tumors 48 hrs after the third mEHT treatment, which was used to detect the amount of hsp70, HMGB1 proteins, and ATP secretion. mEHT treatment resulted in a moderate but significant increase in secreted hsp70 ($p \leq 0.01$), while HMGB1 showed approximately two-fold higher levels ($p \leq 0.004$) and the concentration of ATP was five-fold higher ($p \leq 0.04$) in the treated tumors.

4.9. T-lymphocytes and antigen-presenting cells are increased in mEHT treated lungs

To study the putative contribution of immune cells to tumor growth inhibition by mEHT, we hypothesized that mEHT treatment might result in alteration in the immune status of the lungs and tumor microenvironment. Therefore, we analyzed the expansion of CD3+ T-cells, CD8+ T-cells, and F4/80+CD11b+ macrophage in the lungs of tumor-bearing mice using immunohistochemistry in mEHT-treated and sham-treated animals. Significantly higher CD3+ T-cells infiltration into mEHT-treated tumors was observed compared to sham-treated ones. However, total lung CD3+ T-cells density was comparable between both groups with no statistically significant difference ($p = 0.6037$). In contrast, the differences were significant for CD8+ T-cells, a prominent subtype of CD3+ cells with higher expression of positive cells seen in tumors of mEHT treated lungs ($p = 0.0221$). The total lung CD8+ T-cell density was significantly increased as well in mEHT-treated mice ($p = 0.0238$) compared to the control group. Furthermore, we investigated the density of F4/80+CD11b+ macrophages in tumor and whole lung of mEHT-treated and sham-treated animals. A significantly higher density of F4/80+CD11b+ macrophages was observed in tumors ($p = 0.0363$) and whole lung ($p = 0.0007$) of mice treated with mEHT compared to sham-treated animals.

4.10. mEHT-treated lungs showed no auxiliary lung damage following six-times treatment

To study the potential adverse effect of mEHT treatment on the lungs, we investigated the capability of mEHT to induce significant inflammatory, lung injury, and fibrotic changes in the lungs in both acute and chronic conditions. All mice were treated a total of six times and sacrifice was performed accordingly on day 18 (2 days after last mEHT treatment) and on day 48 (32 days after last mEHT treatment) for acute and chronic cases respectively. To characterize the potential inflammatory effect of mEHT on treated lungs, lung samples were stained for myeloperoxidase (MPO) *via* immunohistochemistry in both mEHT-treated and sham-treated animals for quantification of MPO expressing cells. mEHT induced a significant increase in MPO positive cells under acute conditions compared to the control group ($p = 0.0485$). However, chronic levels of MPO expressing cells measured on day 48, 32 days after the

last treatment showed no significant difference between the groups ($p = 0.2730$), suggesting that the inflammatory impact of mEHT on the lungs is restricted to acute conditions only.

Furthermore, to understand the full spectrum of potential mEHT related adverse effects on mice lungs, we investigated the degree of lung injury in both groups, taking into consideration the scores of each composing parameter, such as cellular infiltrate, alveolar over-distension, atelectasis, interstitial congestion, and hemorrhage. The lung injury score was calculated as the sum of each composing parameters' score. Based on the scores of the composing parameters, we did not observe any significant increase in lung injury following mEHT treatment of mice lungs.

As inflammation can lead to fibrosis, especially under chronic conditions, we assessed the possibility of mEHT-induced fibrotic changes in the lungs by measuring the collagen contents in treated and sham-treated lungs. All samples were Masson's trichrome stained to characterize the collagen contents within the lungs. We did not find any evidence of increased collagen content in the lungs of mEHT-treated animals compared to sham-treated ones in both acute ($p = 0.5381$) and chronic conditions ($p = 0.8927$).

5. Conclusion

In this study, we have demonstrated the capability of mEHT to induce localized heat stress in the lungs, enabled *via* a customized chest electrode designed specifically for targeted treatment of lung tumors while minimizing the dissipation of energy to neighboring tissues and organs in the murine thorax. The verification of pharyngeal-lung temperature quantitative relation enabled the minimally invasive monitoring of lung temperature during treatment of tumor-bearing mice while avoiding any practical adverse effect of direct lung temperature measurement which may involve mechanical lung injury. This technique we believe could offer a particular advantage in clinical settings where accurate estimation of lung temperature is essential to eliminate over-heating or under-treating of primary or metastatic pulmonary cancers with a potential negative impact on treatment outcomes. We have demonstrated that repeated mEHT treatment (at 41.5 – 42.0 °C for 30 min) inhibits the growth of B16F10 melanoma in both primary tumor and pulmonary metastases models. A significant decrease in [^{18}F]FDG uptake and metastatic pulmonary melanoma nodules were observed in the lungs of treated animals.

Upregulation of phosphorylated H2AX was demonstrated with mEHT treatment which led *via* the p53 pathway to upregulation and nuclear localization of $p21^{waf1}$, a potent cyclin-dependent kinase inhibitor responsible for tumor senescence and cell cycle arrest. The downregulating effect of mEHT on Ki67, a prominent tumor proliferation marker, reaffirms its ability to block cell cycle progression in treated tumor cells. Although several mechanisms have been described in this study to play a critical role in the tumor inhibitory effect of mEHT, apoptotic cell death was absent as demonstrated by the insignificant level of CCasp3 expression. As was verified previously in a primary tumor model of B16F10 melanoma, mEHT can induce significant DAMP signal release with the capability to stimulate the anti-tumor immunity that may result in the immunological death of tumor cells. Consequently, an increased density of infiltrating lymphocytes and macrophages was observed in mEHT-treated lungs compared to the sham-treated ones. The massive infiltration of tumors by CD3 and CD8 positive T-lymphocytes and by F4/80 positive macrophages indicated the mobilization of cellular anti-tumor immunity by mEHT. Furthermore, in non-tumor-bearing mice, mEHT treatment-induced lung infiltrating MPO positive cells (primarily neutrophils) was observed only in acute conditions, with insignificant changes of MPO expressing cells observed in chronic conditions. This indicates absent inflammatory changes in the lungs in chronic conditions following mEHT treatment and explains the observed lack of fibrotic pathology in the lungs of treated animals. Despite the obvious therapeutic effects of mEHT treatment on the pulmonary metastases of melanoma as described in this paper, it remains to be evaluated whether synergistic advantages of combining mEHT with already existing treatment modalities may offer a better outcome for patients with primary or metastatic pulmonary cancers.

6. References

1. Younes R, Abrao FC, Gross J. (2013) Pulmonary metastasectomy for malignant melanoma: Prognostic factors for long-term survival. Melanoma Research, 23: 307-311.

2. Tas F. (2012) Metastatic behavior in melanoma: Timing, pattern, survival, and influencing factors. Journal of Oncology, doi:10.1155/2012/647684.

3. Domingues B, Lopes J, Soares P, Populo H. (2018) Melanoma treatment in review. ImmunoTargets and Therapy, Volume 7: 35-49.

4. Kleef R, Moss R, Szasz AM, Bohdjalian A, Bojar H, Bakacs T. (2018) Complete Clinical Remission of Stage IV Triple-Negative Breast Cancer Lung Metastasis Administering Low-Dose Immune Checkpoint Blockade in Combination With Hyperthermia and Interleukin-2. Integrative Cancer Therapies, 17: 1297-1303.

5. Morimoto T, Kimura S, Konishi Y, Komaki K, Uyama T, Monden Y, Kinouchi DY, Iritani DT. (1993) A study of the electrical bio-impedance of tumors. Journal of Investigative Surgery, 6: 25-32.

6. Romero-Garcia S, Moreno-Altamirano MMB, Prado-Garcia H, Sánchez-García FJ. (2016) Lactate contribution to the tumor microenvironment: Mechanisms, effects on immune cells and therapeutic relevance. Frontiers in Immunology, 7: 52.

7. O'Rourke AP, Lazebnik M, Bertram JM, Converse MC, Hagness SC, Webster JG, Mahvi DM. (2007) Dielectric properties of human normal, malignant and cirrhotic liver tissue: in vivo and ex vivo measurements from 0.5 to 20 GHz using a precision open-ended coaxial probe. Physics in medicine and biology, 52: 4707-4719.

8. Cha J, Jeon TW, Lee CG, Oh ST, Yang HB, Choi KJ, Seo D, Yun I, Baik IH, Park KR, Park YN, Lee YH. (2015) Electro-hyperthermia inhibits glioma tumorigenicity through the induction of E2F1-mediated apoptosis. International Journal of Hyperthermia, 31: 784-792.

9. Vancsik T, Forika G, Balogh A, Kiss E, Krenacs T. (2019) Modulated electro-hyperthermia induced p53 driven apoptosis and cell cycle arrest additively support doxorubicin chemotherapy of colorectal cancer in vitro. Cancer Medicine, 8: 4292-4303.

10. Vancsik T, Kovago C, Kiss E, Papp E, Forika G, Benyo Z, Meggyeshazi N, Krenacs T. (2018) Modulated electro-hyperthermia induced loco-regional and systemic tumor destruction in colorectal cancer allografts. Journal of Cancer, 9: 41-53.

11. Meggyeshazi N, Andocs G, Balogh L, Balla P, Kiszner G, Teleki I, Jeney A, Krenacs T. (2014) DNA fragmentation and caspase-independent programmed cell death by modulated electrohyperthermia. Strahlentherapie und Onkologie, 190: 815-822.

12. Overwijk WW, Restifo NP. (2000) B16 as a Mouse Model for Human Melanoma. Current Protocols in Immunology, 39: Unit-Unit.

13. Hofheinz F, Li Y, Steffen IG, Lin Q, Lili C, Hua W, van den Hoff J, Zschaeck S. (2019) Confirmation of the prognostic value of pretherapeutic tumor SUR and MTV in patients with esophageal squamous cell carcinoma. European Journal of Nuclear Medicine and Molecular Imaging, 46: 1485-1494.

14. Shin S, Pak K, Kim IJ, Kim BS, Kim SJ. (2017) Prognostic Value of Tumor-to-Blood Standardized Uptake Ratio in Patients with Resectable Non-Small-Cell Lung Cancer. Nuclear Medicine and Molecular Imaging, 51: 233-239.

15. Hofheinz F, Apostolova I, Oehme L, Kotzerke J, Van Den Hoff J. (2017) Test–retest variability in lesion SUV and lesion SUR in18F-FDG PET: An analysis of data from two prospective multicenter trials. Journal of Nuclear Medicine, 58: 1770-1775.

16. Ehrentraut H, Clambey ET, McNamee EN, Brodsky KS, Ehrentraut SF, Poth JM, Riegel AK, Westrich JA, Colgan SP, Eltzschig HK. (2013) CD73+ regulatory T cells contribute to adenosine-mediated resolution of acute lung injury. FASEB Journal, 27: 2207-2219.

17. Sun X, Bizhanova A, Matheson TD, Yu J, Zhu LJ, Kaufman PD. (2017) Ki-67 Contributes to Normal Cell Cycle Progression and Inactive X Heterochromatin in p21 Checkpoint-Proficient Human Cells. Molecular and Cellular Biology, 37.

18. Al Bitar S, Gali-Muhtasib H. (2019) The Role of the Cyclin Dependent Kinase Inhibitor p21(cip1/waf1) in Targeting Cancer: Molecular Mechanisms and Novel Therapeutics. Cancers (Basel), 11.

19. Fragkos M, Jurvansuu J, Beard P. (2009) H2AX Is Required for Cell Cycle Arrest via the p53/p21 Pathway. Molecular and Cellular Biology, 29: 2828-2840.

20. Podhorecka M, Skladanowski A, Bozko P. (2010) H2AX Phosphorylation: Its Role in DNA Damage Response and Cancer Therapy. J Nucleic Acids, 2010.

7. Bibliography of Candidate's Publications

Publications related to the dissertation

Thomas MJ, Major E, Benedek A, Horváth I, Máthé D, Bergmann R, Szász AM, Krenács T, Benyó Z. (2020) Suppression of metastatic melanoma growth in lung by modulated electro-hyperthermia monitored by a minimally invasive heat stress testing approach in mice. Cancers, 12: 1-24.

Besztercei B, Vancsik T, Benedek A, Major E, **Thomas MJ**, Schvarcz CA, Krenács T, Benyó Z, Balogh A. (2019) Stress-induced, p53-mediated tumor growth inhibition of melanoma by modulated electrohyperthermia in mouse models without major immunogenic effects. International Journal of Molecular Sciences, 20.

Dank M, Balogh A, Benedek A, Besztercei B, Danics LEA, Forika G, Garay T, Hamar P, Karászi Á, Kaucsár T, Kiss É, Krenács T, Major E, Mohácsi R, Portörő I, Ruisanchez É, Schvarcz C, Szász AM, **Thomas JM**, Vancsik T, Zolcsák Z, Benyó Z. (2019) Preclinical and clinical investigation and development of electromag-netic oncological device – experience with solid tumors. Magyar Onkologia, 63: 354-358.

Publications not related to the dissertation

Gaál A, Garay TM, Horváth I, Máthé D, Szöllősi D, Veres DS, **Mbuotidem J**, Kovács T, Tóvári J, Bergmann R, Streli C, Szakács G, Mihály J, Varga Z, Szoboszlai N. (2020) Development and in vivo application of a water-soluble anticancer copper ionophore system using a temperature-sensitive liposome formulation. Pharmaceutics, 12: 466-466.